THE JOURNAL OF Ammonia Energy

Available online at

jae.cardiffuniversitypress.org

ISSN **2752-7735**
The Journal of Ammonia Energy 03 (2025) 103–114

Cardiff University Press | Gwasg Prifysgol Caerdydd

Thermodynamic performance analysis of ammonia synthesis systems based on different electrolyzers

Liu L[a], Zhang H[a,*], Zhang Y[a], Baldinelli A[b], Sun M[a], Nian X[a], Duan L[a], Desideri U[b]

[a] *School of Energy, Power and Mechanical Engineering, North China Electric Power University, Beijing, China*
[b] *University of Pisa, Department of Energy, Systems, Territory and Constructions Engineering, Pisa, Italy*

Abstract

To avoid greenhouse gas emissions, reduce the dependence of the traditional ammonia synthesis process on fossil energy, and achieve a low-carbon and sustainable transformation of the ammonia synthesis process, the electrolyzer-based ammonia synthesis system has gradually attracted people's attention. This paper compares and analyses the thermodynamic performance of the synthetic ammonia system when operating with different electrolyzers: alkaline water electrolyzer (AWE), proton exchange membrane electrolyzer (PEMEC), and solid oxide electrolyzer (SOEC). The results show that the energy efficiency of the synthetic ammonia system based on AWE, PEMEC and SOEC is 54.99%, 59.94%, and 77.19%, respectively, which is in positive correlation with the hydrogen production efficiency of the electrolyzer. Meanwhile, by comparing the heat integration of different synthetic ammonia systems, it is found that the heat integration processes of synthetic ammonia systems based on PEMEC and AWE are identical because the excess heat from the low-temperature electrolyzer is directly discharged to the environment through cold utilities, which means that the synthetic ammonia system can adopt the PEMEC and AWE collaborative hydrogen production solution to achieve a trade-off between system flexibility and economy. The high-temperature electrolyzer (SOEC) exhibits the advantage of high thermodynamic compatibility with ammonia synthesis reactions, enabling more efficient utilization of system waste heat and further enhancing the overall system efficiency.

Received: 18th Dec 24; Accepted: 24st Mar 25; Published: 11th Apr 25

Keywords: Green ammonia, Green hydrogen, Pinch analysis, Energy integration.

1. Introduction

To achieve the green and sustainable development of the energy supply system, the installed capacity of renewable energy, mainly wind power and photovoltaics, is constantly increasing. While reducing carbon emissions, it cannot guarantee the stability of the power supply due to its randomness and volatility. Therefore, developing large-capacity, long-term energy storage technology has become key to developing renewable energy. In this context, the energy storage concept of Power to X has received widespread interest since it not only solves the problem of renewable energy consumption but also promotes energy conservation and emission reduction in traditional chemical production based on fossil energy, where X includes hydrogen, ammonia, methanol, methane, etc. [1–3]. Compared to other chemical products, ammonia, the second largest chemical product in the world, has the unique properties of low-ignition point, producing only nitrogen and hydrogen when decomposed, and no carbon dioxide emissions [4,5]. It is regarded as an ideal chemical for long-term hydrogen storage.

The differences in thermodynamic performance between electrolyzer-based ammonia synthesis systems and traditional ammonia synthesis processes have attracted the attention of many scholars. Bahnamiri et al. [6] put forward a system for the co-production of ammonia and formic acid based on alkaline water electrolyzer (AWE) and CO_2 electroreduction cells. The system efficiency reached 37.6%, while CO_2 recycling was achieved. However, the study only focused on the impact of changes in key component parameters on the thermodynamic performance of the system. Sousa et al. [7] investigated the technical and economic trade-off of the ammonia synthesis system based on proton exchange membrane electrolyzer (PEMEC). It is reported that the energy efficiency is 45%, and the energy consumption of ammonia production was 10.98kWh/kg NH_3, which is 2 kWh/kg NH_3 greater than the energy consumption of the typical natural gas reforming ammonia synthesis system. It was also pointed out that when electricity costs are low, the system should reduce investment costs and shorten the system investment payback period by increasing the PEMEC current density at the expense of the electrolyzer hydrogen production efficiency. Richard et al. [8] explored the potential

* Corresponding author. Tel.: +86 18911079664 E-mail address: hanfei.zhang@ncepu.edu.cn
https://doi.org/10.18573/jae.43

of adopting PEMEC or SOEC to produce hydrogen and using membrane reactors to synthesize ammonia. The study employed a multi-objective optimization algorithm to optimize system operating parameters to minimize ammonia production costs and improve system efficiency. The study found that the use of membrane technology can achieve an ammonia conversion rate of up to 90% compared to traditional ammonia synthesis. In addition, the efficiency of membrane reactor ammonia synthesis systems based on PEMEC and SOEC increased by approximately 8% and 15%, respectively. However, the above studies only focus on the impact of key system operating parameters on system efficiency and economy or explore the trade-off between technology and economics, and lack discussion on the utilization of system waste heat and the system-level energy integration. For the ammonia synthesis system of SOEC and solid oxide electrolyte oxygen pump, Nowicki et al. [9] pointed out that if the waste heat of the solid oxide electrolyte oxygen pump can be further utilized, the energy consumption of the ammonia synthesis system can be further improved on the basis of 9.94 kWh/kg NH_3. Frattini et al. [10] evaluated the performance of biomass-based, electrolyzer-based, biogas-based, and natural gas-based ammonia synthesis systems. The findings indicated that the global efficiency of the electrolyzer-based system was as high as 81%, the energy consumption of ammonia production was 14.36 kWh/kg NH_3, They also pointed out that the large amount of waste heat from the ammonia synthesis reactor and multi-stage compressor in the three systems can be further recovered and utilized for heating or providing domestic hot water. Nami et al. [11] conducted a technical and economic analysis of the synthetic ammonia systems based on AWE and solid oxide electrolyzer (SOEC). It is concluded that the energy efficiency of the ammonia synthesis systems based on low-temperature and high-temperature AWE, and low-pressure and high-pressure SOEC are 56.4%, 66%, 72.5%, and 73.4%, respectively. In addition, in the system based on low-pressure and high-pressure SOEC, around 57% and 31% of the steam required by the electrolyzer can be obtained by heat integration between the SOEC and the Haber-Bosch process, respectively. Zhou et al. [12] conducted the PEMEC and SOEC-based ammonia synthesis systems with the pinch analysis method, pointing out that the heat generated by the ammonia synthesis system based on PEMEC can be self-sufficient and does not require additional thermal utilities, while the hydrogen production and ammonia synthesis system of SOEC requires an additional 35.1MW of steam to meet the system's heat demand. However, there is a lack of comparative analysis between ammonia synthesis systems based on low-temperature electrolyzers (PEMEC and AWE).

Meanwhile, the pinch point analysis method optimizes the system heat exchange network design by determining the minimum temperature difference (pinch point) between the cold and hot flows in the system. It can maximize the recovery of system waste heat, reduce the system's demand for external energy, and achieve the lowest system energy consumption. It is an important method to achieve system-level energy integration in process system engineering. Therefore, to fill the above research gap, this paper uses the pinch analysis method and the combination curve to visualize the integration process of different logistics when the synthetic ammonia system adopts different hydrogen production technologies and compares the integration characteristics and energy-saving potential of different hydrogen production technologies in the synthetic ammonia system.

Nomenclature

AWE	alkaline water electrolyzer	V	voltage, V
ASP	ammonia synthesis process	W	electricity, kW
ASU	air separation unit	ρ	catalyst volume density
COMP	compressor		
COP	coefficient of performance	Superscripts and subscripts	
GSR	gas switching reforming	a	anode
HEX	heat exchanger	act	activation
MCOMP	multi-stage compressor	c	cathode
PEMEC	proton exchange membrane electrolyzer	cat	catalyst
R717	refrigeration unit	en	energy
SOEC	solid oxide electrolyzer	inv	investment
Sep	separator	ion	ionic
Symbols		ocv	open circuit voltage
j	the current density of electrolyzer, A/cm^2	ohm	ohmic

2. Process description

The flowchart of the ammonia synthesis system based on the electrolyzer is given in Fig. 1. First, water is transformed in the electrolyzer to produce hydrogen and oxygen, which are then separated by a gas-liquid separator (Sep 1 and Sep 2) to obtain pure hydrogen (stream 6) and pure oxygen (stream 10). Subsequently, the oxygen (stream 10) produced by the electrolyzer is blended with the oxygen from the cryogenic air separation unit (ASU) and sold. In contrast, the hydrogen generated from the electrolyzer cooled by a heat exchanger (HEX 2) is mixed with the nitrogen from the ASU in a ratio of 3:1 and enters a multi-stage compressor (Mcomp3) for compression. The mixed gas (stream 20) is then mixed with the unreacted gas (stream 32) separated from the ammonia separation tower (Sep 3) and enters a compressor (Comp) for further compression to the operating pressure of the synthetic ammonia reactor. As the ammonia synthesis process is exothermic and the conversion efficiency of nitrogen and hydrogen is low, the ammonia synthesis reactor in this paper adopts a three-bed reactor to improve the conversion rate of nitrogen and hydrogen while achieving temperature control. Specifically, the mixed gas from the compressor is first heated to about 180 ℃ to prevent the cooling temperature entering the reaction bed from being too low, which would affect the catalyst performance. Then, stream 22 is split into three streams, the first stream (stream 23) is further heated to the operating temperature of the synthetic ammonia reactor through the HEX 5, and the second (stream 25) and third (stream 26) streams are passed into the ammonia synthesis reactor as cooling gas to manage the reaction temperature and prevent the reactor temperature from being too high and affecting the synthetic ammonia reaction. The crude synthesis gas (stream 27) from the synthetic ammonia reactor is cooled by the HEX6, enters a refrigeration unit (R717) to liquefy the ammonia, and then enters the ammonia separation towers (Sep 3 and Sep 4) to yield pure ammonia (stream 36). Finally, some unreacted gas (stream 25 and stream 26) is separated and sent to the boiler for combustion.

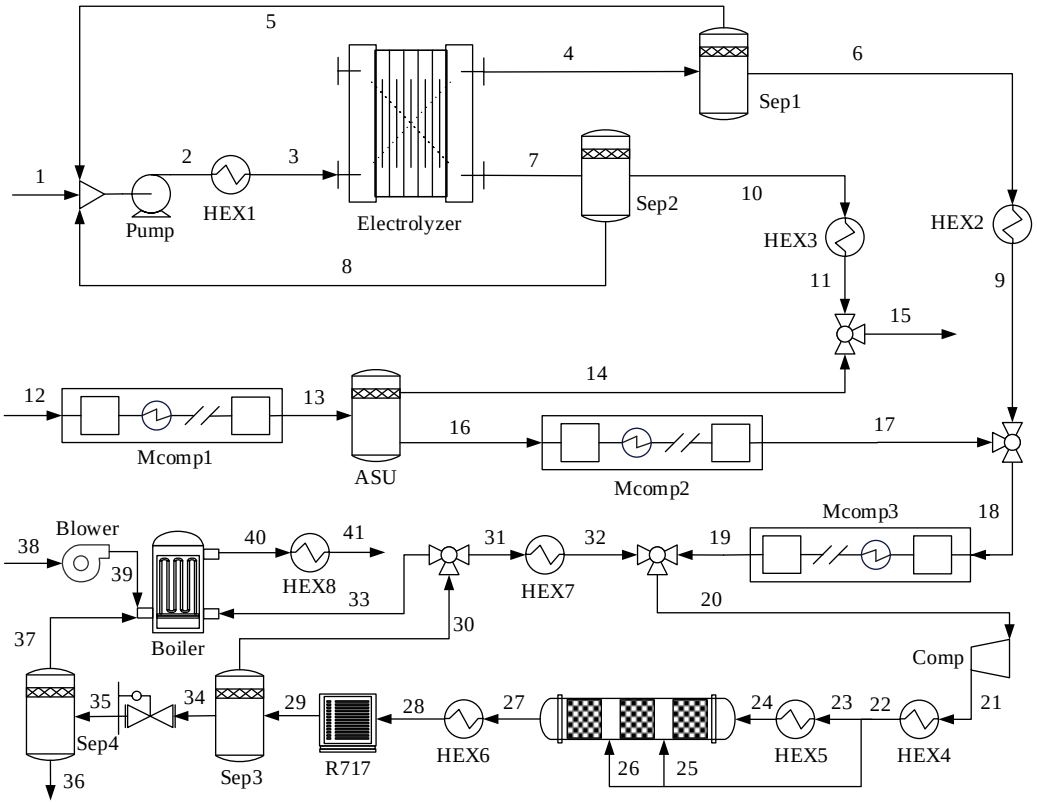

Fig. 1. The flowchart of ammonia synthesis system

3. System modeling

3.1 AWE model

In the alkaline electrolyte solution, the alkaline water electrolyzer separates the anode and cathode through a diaphragm and water undergoes electrochemical reactions at the cathode and anode to produce hydrogen and oxygen respectively. The reaction equations are as follows:

Overall reaction:

$$H_2O \rightarrow H_2 + \frac{1}{2}O_2 \quad (1)$$

Anode reaction:

$$2OH^- \rightarrow 2e^- + H_2O + \frac{1}{2}O_2 \quad (2)$$

Cathode reaction:

$$2H_2O + 2e^- \rightarrow H_2 + 2OH^- \quad (3)$$

Taking into account the kinetic and resistance effects during the operation of the electrolyzer, the actual operating voltage of the AWE is the sum of the reversible voltage, activation overpotential, and ohmic overpotential [13,14]. As detailed in Table 1 where T_{AWE} is the AWE working temperature, ℃; p_{AWE} is the AWE working pressure, bar; j_{AWE} is the AWE working current density, A/m^2; The parameters of the AWE model [13] are described in the supplement material. As illustrated in Fig. 2, under the same operating parameters, the voltage of the AWE model at different current density was compared with reference [13], and it is found that the absolute value of error is less than 0.2%, which proved the reliability of the model.

Table 1. The modeling equations of AWE.

Parameters	Equations
AWE cell voltage, V	$V_{AWE} = V_{rev} + V_{AWE,act} + V_{AWE,ohm}$
Activation overpotential, V	$V_{AWE,act} = S \cdot \log\left[\left(t_1 + \frac{t_2}{T_{AWE}} + \frac{t_3}{T_{AWE}^2}\right) \cdot j_{AWE} + 1\right]$
Ohmic overpotential, V	$V_{AWE,ohm} = j_{AWE} \cdot \left[\left(r_1 + d_1\right) + r_2 \cdot T_{AWE} + d_2 \cdot p_{AWE}\right]$
Faraday efficiency	$\eta_{Faraday,AWE} = \left(\frac{j_{AWE}^2}{f_1 + f_2 \cdot T_{AWE} + j_{AWE}^2}\right) \cdot \left(f_3 + f_4 \cdot T_{AWE}\right)$
Hydrogen production, mol/s	$n_{AWE,H_2} = \eta_{Faraday,AWE} \cdot \frac{j_{AWE} \cdot A_{AWE,cell}}{2 \cdot F} N_{AWE,cell}$
Oxygen production, mol/s	$n_{AWE,O_2} = \frac{1}{2} n_{AWE,H_2}$
Water consumed	$n_{AWE,H_2O} = n_{AWE,H_2}$
Power consumption, kW	$W_{AWE,stack} = j_{AWE} \cdot A_{AWE,cell} \cdot N_{AWE,cell} \cdot V_{AWE}$
Energy efficiency	$\eta_{en,AWE} = \frac{n_{AWE,H_2} \cdot LHV_{H_2}}{W_{AWE,stack}}$

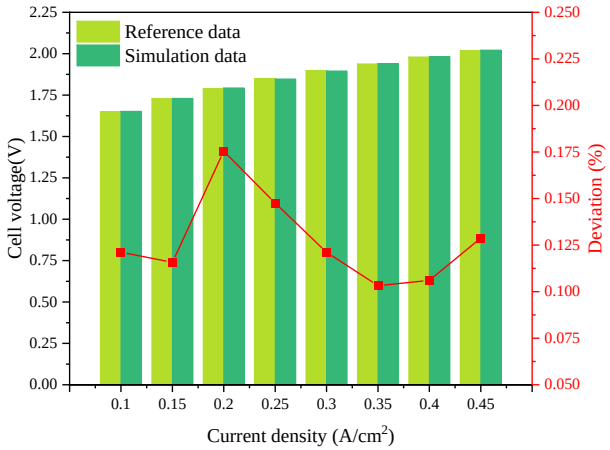

Fig. 2. The comparison of experimental data and simulated data of the AWE model.

Overall reaction:

$$H_2O \rightarrow H_2 + \frac{1}{2}O_2 \quad (4)$$

Anode reaction:

$$H_2O \rightarrow 2H^+ + \frac{1}{2}O_2 + 2e^- \quad (5)$$

Cathode reaction:

$$2H^+ + 2e^- \rightarrow H_2 \quad (6)$$

The proton exchange membrane electrolyzer's voltage consists of open-circuit, activation, ohmic, and concentration voltage. The concentration voltage is omitted in the model because it is much smaller than the other voltages[15,16]. The formula to calculate the voltage is shown in **Table 2**.

3.2 PEMEC model

The electrochemical reactions occurring in PEMEC are as follows:

Table 2. The modeling equations of PEMEC.

Parameters	Equations
PEMEC voltage, V	$V_{\mathrm{PEMEC}} = V_{\mathrm{PEMEC,ocv}} + V_{\mathrm{PEMEC,act}} + V_{\mathrm{PEMEC,ohm}}$
Open-circuit voltage, V	$V_{\mathrm{PEMEC,ocv}} = 1.229 - 0.9\times10^{-3}\left(T_{\mathrm{PEMEC}} - 298\right) + \frac{\mathrm{R}T_{\mathrm{PEMEC}}}{2\mathrm{F}}\ln\left(\frac{p_{\mathrm{H_2}} \cdot p_{\mathrm{O_2}}^{0.5}}{P_{\mathrm{H_2O}}}\right)$
Activation overvoltage, V	$V_{\mathrm{PEMEC,act}} = \frac{\mathrm{R}T_{\mathrm{PEMEC}}}{\alpha_{\mathrm{a}}\mathrm{F}}\sinh^{-1}\left(\frac{j_{\mathrm{PEMEC}}}{2j_{0,\mathrm{a}}}\right) + \frac{\mathrm{R}T_{\mathrm{PEMEC}}}{\alpha_{\mathrm{c}}\mathrm{F}}\sinh^{-1}\left(\frac{j_{\mathrm{PEMEC}}}{2j_{0,\mathrm{c}}}\right)$
Ohmic overvoltage, V	$V_{\mathrm{PEMEC,ohm}} = j_{\mathrm{PEMEC}}\left(\frac{\delta_{\mathrm{m}}}{\sigma_{\mathrm{m}}} + R_{\mathrm{ele}}\right)$
Membrane conductivity, S/m	$\sigma_{\mathrm{m}} = \left(0.005139\lambda_{\mathrm{m}} - 32.6\right)\cdot\exp\left[1268\left(\frac{1}{303} - \frac{1}{T_{\mathrm{PEMEC}}}\right)\right]$
Hydrogen production, mol/s	$n_{\mathrm{PEMEC,H_2}} = \eta_{\mathrm{Faraday,PEMEC}} \cdot \frac{j_{\mathrm{PEMEC}} \cdot A_{\mathrm{PEMEC,cell}}}{2\cdot\mathrm{F}} N_{\mathrm{PEMEC,cell}}$
Oxygen production, mol/s	$n_{\mathrm{PEMEC,O_2}} = \frac{1}{2}n_{\mathrm{PEMEC,H_2}}$
Water consumed, mol/s	$n_{\mathrm{PEMEC,H_2O}} = n_{\mathrm{PEMEC,H_2}}$
Power consumption, kW	$W_{\mathrm{PEMEC,stack}} = j_{\mathrm{PEMEC}} \cdot A_{\mathrm{PEMEC,cell}} \cdot N_{\mathrm{PEMEC,cell}} \cdot V_{\mathrm{PEMEC}}$
Energy efficiency	$\eta_{\mathrm{en,PEMEC}} = \frac{n_{\mathrm{PEMEC,H_2}} \cdot \mathrm{LHV}_{\mathrm{H_2}}}{W_{\mathrm{PEMEC,stack}}}$

Where T_{PEMEC} is the PEMEC working temperature, K; j_{PEMEC} indicates the PEMEC current density, A/cm^2; $j_{0,\mathrm{a}}$ and $j_{0,\mathrm{c}}$ denote the cathode and anode exchange current densities, respectively, A/cm^2; $A_{\mathrm{PEMEC,cell}}$ is the active area of the electrolytic cell, cm^2; According to reference [17,18], the other variables of the PEMEC model have been described in the supplement material. As shown in Fig. 3, the absolute value of the error between the voltage of the PEMEC model at different current densities and the literature data[19] is within an acceptable range (<1%), demonstrating the accuracy of the model.

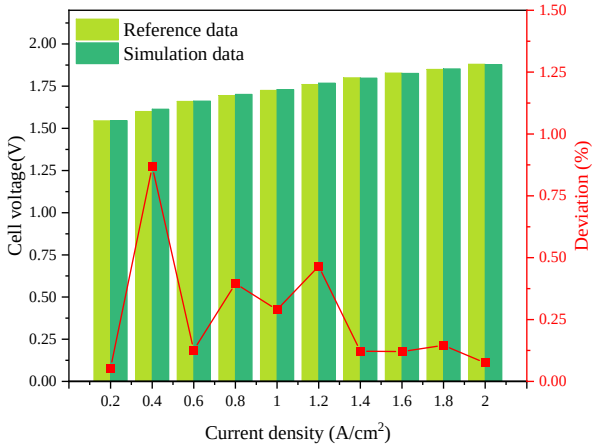

Fig. 3. The comparison of experimental data and simulated data of the PEMEC model.

3.3 SOEC model

Unlike low-temperature electrolyzers (PEMEC and AWE), for high-temperature SOEC, water vapor is transformed into hydrogen and oxygen, which reduces the activation energy of the water decomposition reaction and further improves the efficiency of hydrogen production by electrolysis. The reaction equations at the anode and cathode are as follows,

Overall reaction:

$$H_2O \rightarrow H_2 + \frac{1}{2}O_2 \quad (7)$$

Anode reaction:

$$O^{2-} - 2e^- \rightarrow \frac{1}{2}O_2 \quad (8)$$

Cathode reaction:

$$H_2O + 2e^- \rightarrow H_2 + O^{2-} \quad (9)$$

According to the literature, the voltage of SOEC is the sum of Nernst potential, activation overpotential of anode and cathode, ohmic overpotential, and the overpotential related to interconnect, and Table 3 shows the detailed SOEC modeling process [20,21]. Where T_{SOEC} is the SOEC working temperature, K; p_{SOEC} is the SOEC working pressure, bar; Z_{H_2}, Z_{O_2} and Z_{H_2O} are the mole fraction of H_2, O_2, and H_2O, respectively; β is the electrode asymmetry charge transfer coefficient.

Table 3. The modeling equations of SOEC.

Parameters	Equations
SOEC cell voltage, V	$V_{SOEC} = V_{SOEC} + V^{a}_{SOEC,act} + V^{c}_{SOEC,act} + V_{SOEC,ohm} + V_{SOEC,mic}$
Nernst potential, V	$V_{nern} = 1.20672 - 2.87902\times10^{-4}\times T_{SOEC} + \frac{RT_{SOEC}}{2F} * ln\left(\frac{Z_{H_2} * (p_{SOEC} * Z_{O_2})^{0.5}}{Z_{H_2O}}\right)$
Cathode activation overpotential, V	$j_{H_2} = j_{0,H_2}\left(exp\left(\frac{(1+\beta_a)FV^{c}_{SOEC,act}}{RT_{SOEC}}\right) - exp\left(\frac{\beta_c FV^{c}_{SOEC,act}}{RT_{SOEC}}\right)\right)$
Anode activation overpotential, V	$j_{O_2} = j_{0,O_2}\left(exp\left(\frac{\beta_a FV^{a}_{SOEC,act}}{RT_{SOEC}}\right) - exp\left(-\frac{\beta_c FV^{a}_{SOEC,act}}{RT_{SOEC}}\right)\right)$
Ohmic overpotential related to electrolyte, V	$j_i = \frac{V_{ohm,i}}{\delta_e}\left(\frac{k_e}{T_{SOEC}} e^{-\frac{E_e}{RT_{SOEC}}}\right)$
Ohmic overpotential related to interconnect, V	$j_i = \frac{V_{mic,i}}{\delta_{mic}}\left(\frac{k_{mic}}{T_{SOEC}} e^{-\frac{E_{mic}}{RT_{SOEC}}}\right)$
Hydrogen production, mol/s	$n_{SOEC,H_2} = \eta_{Faraday,SOEC} \cdot \frac{j_{SOEC} \cdot A_{SOEC,cell}}{2 \cdot F} N_{SOEC,cell}$
Oxygen production, mol/s	$n_{SOEC,O_2} = \frac{1}{2} n_{SOEC,H_2}$
Water consumed	$n_{SOEC,H_2O} = n_{SOEC,H_2}$
Power consumption, kW	$W_{SOEC,stack} = j_{SOEC} \cdot A_{SOEC,cell} \cdot N_{SOEC,cell} \cdot V_{SOEC}$
Energy efficiency	$\eta_{en,SOEC} = \frac{n_{SOEC,H_2} \cdot LHV_{H_2}}{W_{SOEC,stack}}$

Other parameters include j_i, which is the current density attributed to the active species i, A/cm^2; k_e and k_{mic} are the pre-exponential factor, respectively, S K/m; E_e and E_{mic} are the activation energy of the electrolyte and interconnect, respectively, J/mol; δ_e and δ_{mic} are the thickness of the electrolyte and interconnect, m. The parameters of the SOEC model are described in the supplement material according to reference [21,22].

3.4 Ammonia synthesis model

The Haber-Bosch process is the primary industrial approach for synthesizing ammonia. In the ammonia synthesis reactor, hydrogen from the electrolyzer and nitrogen from the ASU are mixed in a ratio of 3:1 to synthesize ammonia under the conditions of iron-based catalyst, 450-600℃, and 100-250 bar [20]. The reaction equation is shown as follows:

$$\frac{1}{2}N_2 + \frac{3}{2}H_2 = NH_3 \quad (10)$$

The Temkin-Pyzhev kinetic model is adopted to illustrate the reaction kinetics of the ammonia synthesis process [23].

$$R_{NH_3} = \frac{2f}{\rho_{cat}}\left(k_1 \frac{p_{N_2} p_{H_2}^{1.5}}{p_{NH_3}} - k_{-1}\frac{p_{NH_3}}{p_{H_2}^{1.5}}\right) \quad \left(\frac{\text{kmol NH}_3}{\text{kg}_{cat}.\text{h}}\right) \quad (11)$$

$$k_1 = 1.79\times10^4 e^{-87090/RT} \quad (12)$$

$$k_{-1} = 2.75\times10^{16} e^{-198464/RT} \quad (13)$$

where ρ_{cat} is the volume density of the catalyst, kg/m^3; f represents the correction factor, 4.75; p_i represent the pressure of the related gas, bar.

3.5 Other models

The air separation process is simulated using a typical double-tower cryogenic air separation model from Aspen Plus. The comprehensive power consumption of cryogenic air separation is 0.4 kWh/Nm^3 O_2. The ammonia refrigeration unit in the synthetic ammonia process is treated as a black box with a COP of 2.14 [24]. Meanwhile, the heat exchanger model and the steam turbine cycle in the heat recovery subsystem have been described in the literature [25].

4. Thermodynamic performance evaluation indicators

To assess the effectiveness of the system's energy conversion, energy and exergy efficiencies are selected[20,26], which can be calculated as follows:

$$\eta_{en} = \frac{m_{NH_3}\cdot \text{LHV}_{NH_3}}{W_{net}} \quad (14)$$

$$\eta_{ex} = \frac{m_{NH_3}\cdot \text{Ex}_{NH_3}}{W_{net}} \quad (15)$$

Where W_{net} is the net power consumed by the system to synthesize ammonia, kW. Table 4 shows the ammonia synthesis system design parameters. The steam pressure level 1, 2, and 3 represent the high, medium, and low pressure drum pressures of the waste heat recovery subsystem, respectively. The superheat represents the superheat of the steam at the corresponding drum pressure.

Table 4. Design parameters of the synthetic ammonia system.

Parameters	Value
Ammonia synthesis pressure, bar	200
AWE operating pressure, bar	10
AWE operating temperature, ℃	80
PEMEC operating pressure, bar	10
PEMEC operating temperature, ℃	80
SOEC operating pressure, bar	10
SOEC operating temperature, ℃	750
Steam pressure level 1, bar	120
Steam pressure level 2, bar	65
Steam pressure level 3, bar	1
Steam superheat, ℃	250

5. Results and discussion

5.1 Thermodynamic Performance Analysis

The material and energy balance of the AWE-based ammonia synthesis system is shown in Fig. 4. When the ammonia production is 6.944 kg/s, the byproduct oxygen production is 11.836 kg/s, of which 14.75% comes from the cryogenic air separation unit, and 85.25% comes from the electrolyzer. The comparative thermodynamic performance of synthetic ammonia systems based on different electrolyzers in **Error! Reference source not found.** shows that the energy and exergy efficiency of the AWE-based ammonia synthesis system are 51.67% and 54.99%, respectively. The total power consumption is 259.09MW, and the Steam Rankine Cycle generates 9.4MW of electricity by absorbing the system's waste heat, making the system's net power consumption 249.69MW.

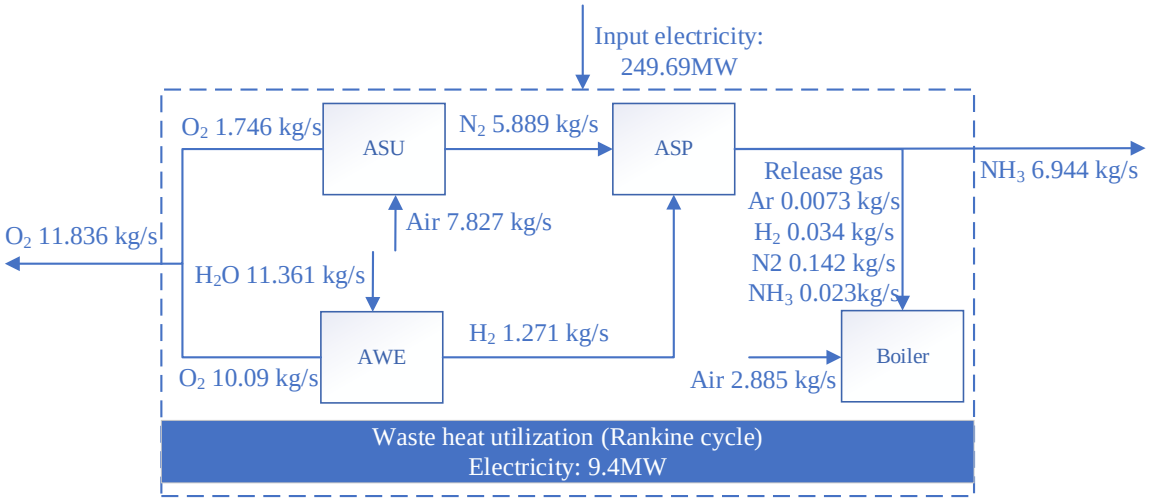

Fig. 4. Material and energy balance of AWE-based ammonia synthesis system.

In addition, to avoid the accumulation of inert gases in the ammonia synthesis process and to avoid affecting the progress of the ammonia synthesis reaction, some unreacted gases (0.0073 kg/s Ar; 0.0034 kg/s H_2, 0.142 kg/s N_2, 0.023 kg/s NH_3) are discharged during ammonia separation and sent to the waste heat boiler for combustion to recover part of the energy in the mixed gas.

Figure 5 shows the material energy balance of the PEMEC-based synthetic ammonia system. The system has a net power consumption of 229.06 MW, with energy and exergy efficiencies of 56.32% and 59.94% respectively since the hydrogen production efficiency of PEMEC is higher than that of AWE. Meanwhile, as both PEMEC and AWE are low-temperature electrolyzers, there is no need to provide additional heat to the electrolyzer and the operating parameters of the system Rankine cycle remain unchanged. Hence, the Rankine cycle of the two ammonia synthesis systems generates 9.4 MW of electricity.

The material and energy balance of the SOEC-based ammonia synthesis system is illustrated in Fig. 6. In contrast to low-temperature electrolyzers, SOEC directly electrolyzes water vapor to produce hydrogen and oxygen, reducing the Gibbs free energy of water decomposition. The electrolyzer's hydrogen production efficiency has been improved. With the same ammonia yield and Rankine cycle parameters, the energy and exergy efficiencies of the system are further enhanced to 72.53% and 77.19% respectively. Meanwhile, SOEC needs to absorb waste heat in the system to generate steam for electrolysis, which reduces the amount of steam in the Rankine cycle, resulting in the power generation of the Rankine cycle being only 3.67MW, which is 39.04% of the power generated by the Rankine cycle of the first two synthetic ammonia systems. However, due to the higher hydrogen production efficiency of SOEC (>90%), the total and net power consumption of the system are still the lowest, at 181.53MW and 177.86MW respectively, and the net power consumption is 71.23%, and 77.65% of the AWE and the PEMEC-based synthetic ammonia system, respectively. The supplementary material in the appendix provides more detailed mass and energy balance information for the system.

5.2 System heat integration

The grand composite curve of the system provides a clear view of the distribution of the heat load in different temperature ranges and the heat exchange pinch point temperature of the system. As illustrated in Fig. 7, it is the grand composite curve of the AWE-based ammonia synthesis system. According to the meaning of the grand composite curve: (1) Temperatures higher than the pinch point temperature represent heat trap for the system and only require hot utilities; (2) Temperatures lower than the pinch point represent heat source for the system and only require cold utilities; (3) The slope of the grand composite curve in different temperature ranges represents the inverse of the heat capacity flow rate after the integration of the cold and hot streams. Specifically, a positive slope indicates that there is insufficient heat after integrating the cold and hot streams, and a negative slope means excess heat after integrating the cold and hot streams. The following conclusions can be drawn by analyzing Fig. 7.

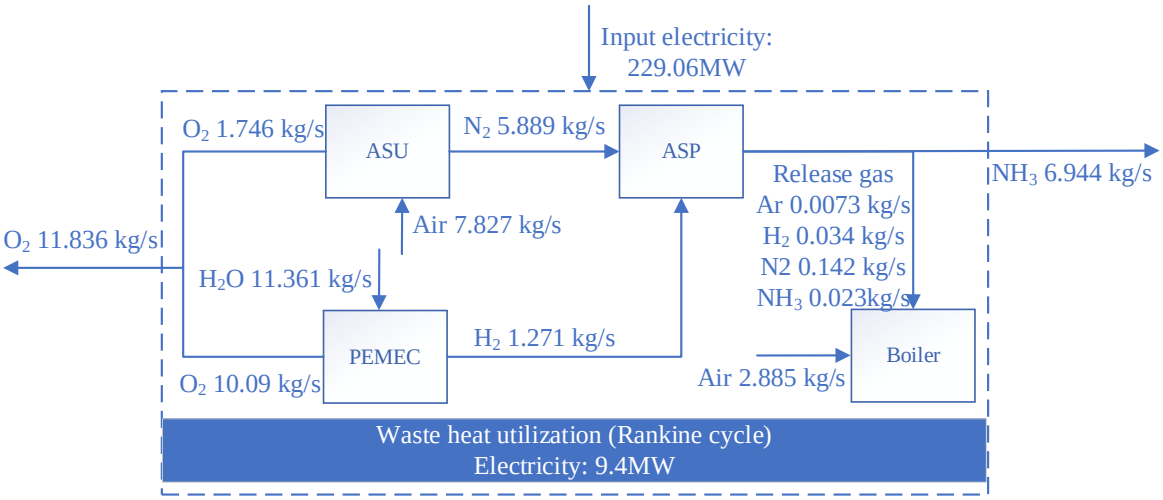

Fig. 5. Material and energy balance of the PEMEC-based ammonia synthesis system.

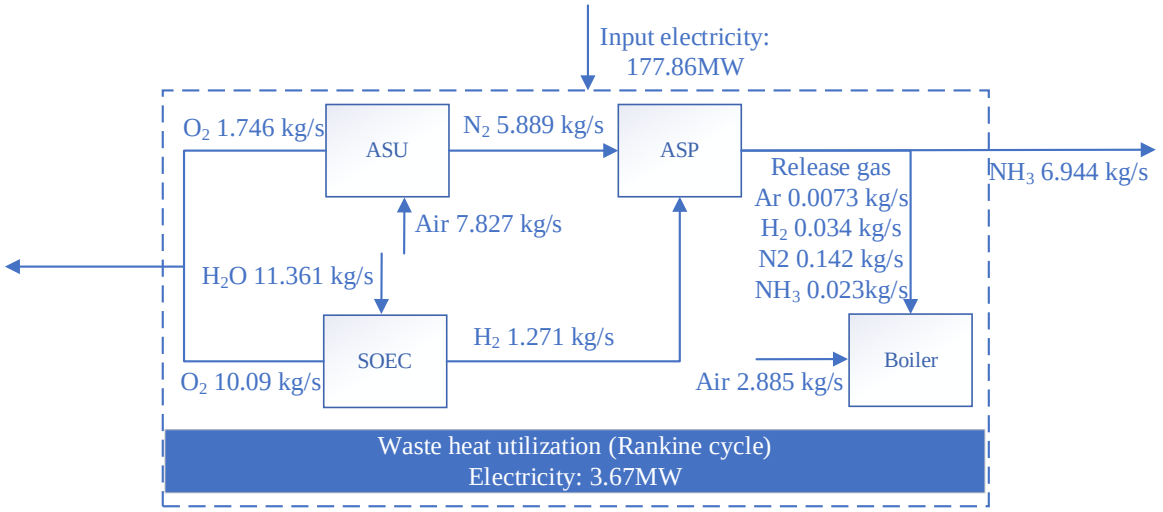

Fig. 6. Material and energy balance of the SOEC-based ammonia synthesis system.

Table 5. Comparison of thermodynamic performance of ammonia synthesis systems based on different electrolyzers.

Parameters	AWE	PEMEC	SOEC
Ammonia production, kg/s	6.944	6.944	6.944
Total power consumption, MW	259.09	238.46	181.53
Net power consumption, MW	249.69	229.06	177.86
Electrolyzer power consumption, MW	242.36	221.73	164.8
ASU power consumption, MW	1.79	1.79	1.79
ASP power consumption, MW	14.94	14.94	14.94
Rankine cycle power generation, MW	9.4	9.4	3.67
Energy efficiency, %	51.66	56.32	72.53
Exergy efficiency, %	54.99	59.94	77.19

The pinch point temperature in the heat exchange network of the AWE-based synthetic ammonia system is 486.1 ℃; above the pinch point temperature, the system does not require hot utility. The heat exchange process is mainly for the high-temperature flue gas from the boiler to heat the superheated steam in the Rankine cycle. Below the pinch point temperature, the raw synthesis gas leaving the ammonia synthesis reactor and the flue gas from the boiler release heat together to heat the saturated steam in the steam Rankine cycle and the mixed gas to the ammonia synthesis reactor, respectively. When the temperature is below 100 ℃, the low-temperature waste heat generated by the AWE, flue gas, compressors, condenser, etc. in the system is discharged to the environment through cold utility.

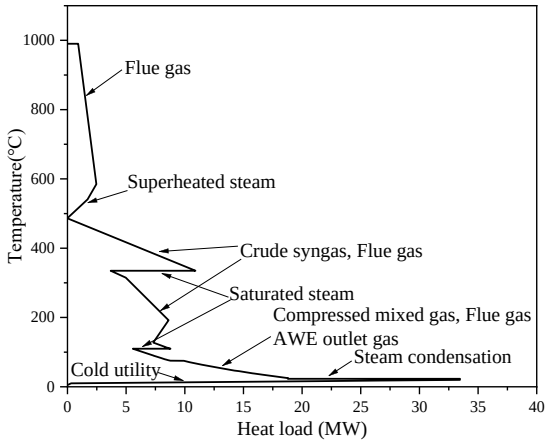

Fig. 7. Grand composite curve of ammonia synthesis system based on AWE.

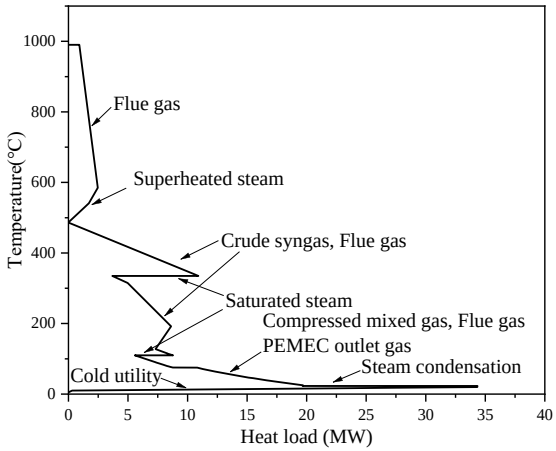

Fig. 8. Grand composite curve of ammonia synthesis system based on PEMEC.

As illustrated in Fig. 8, it is the grand composite curve of the ammonia synthesis system based on PEMEC. Since PEMEC and AWE are both low-temperature electrolyzers with similar operating temperatures, the grand composite curve of the ammonia synthesis system based on PEMEC is identical, the pinch point temperature is also 486.1 ℃, and the heat exchange process of the system's hot and cold stream is the same, so it will not be described in detail.

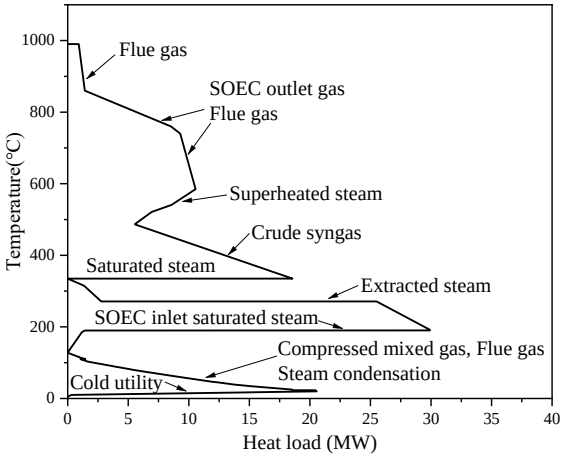

Fig. 9. Grand composite curve of ammonia synthesis system based on SOEC.

The grand composite curve of the ammonia synthesis system based on SOEC is shown in Fig. 9.It is different from the grand composite curve of the AWE-based and PEMEC-based synthetic ammonia system, under the same Rankine cycle parameters; there are two pinch point temperatures in the system grand composite curve, which are 128.2 ℃ and 334.8 ℃ respectively, and the system does not require the hot utility. When the stream temperature is higher than 334.8 ℃, the heat exchange process in the system is mainly the high-temperature flue gas from the boiler, the outlet gas of the SOEC, and the syngas at the outlet of the synthetic ammonia reactor heating the superheated steam and saturated steam of the Rankine cycle. When the stream temperature is between 128.2℃ and 334.8℃, part of the steam in the Rankine cycle is extracted to heat the saturated steam at the inlet of the SOEC. When the stream temperature is lower than 128.2℃, the low-temperature waste heat from the SOEC outlet, compressed gas, flue gas, and condenser in the system is directly discharged to the environment through the cold utility.

6. Conclusions

In this paper, the system energy and exergy efficiency are selected as assessment criteria, and the thermodynamic performances of synthetic ammonia systems based on different electrolyzers are compared. The heat exchange process between different streams in the system is discussed through the system's heat integration. The key conclusions are summarised as follows,

(1) The energy efficiency of the synthetic ammonia systems based on AWE, PEMEC, and SOEC are 51.66%, 56.31%, and 72.53% respectively. The synthesis system efficiency is positively correlated

with the hydrogen production efficiency of the electrolyzer because the hydrogen production efficiency directly affects the power consumption of the system;

(2) the heat exchange pinch point temperature of the synthetic ammonia system based on AWE and PEMEC is 486.1℃. Since the electrolyzer is low-temperature, the low-temperature waste heat from the electrolyzer is directly discharged to the environment through the cold utility. It does not affect the heat integration. Therefore, the heat integration process of the synthetic ammonia system of the low-temperature electrolyzer is similar;

(3) when the synthetic ammonia system adopts SOEC to produce hydrogen and the operating parameters of the Rankine cycle remain unchanged, there are two pinch point temperatures in the synthetic ammonia system, which are 128.2℃ and 334.8℃ respectively. To reduce the temperature difference between the heat exchange streams, the waste heat in the system will prioritize heating the steam in the Rankine cycle. When the Rankine cycle steam temperature drops to 281℃ due to work, part of the steam is extracted to heat the saturated steam at the SOEC inlet. Similarly, the low-temperature waste heat in the system below 128.2℃ is directly discharged to the environment through the cold utility.

In conclusion, since SOEC is still in the laboratory research stage, there is a complementary relationship between the load response of PEMEC and the economic efficiency of AWE, and the low-temperature waste heat generated by PEMEC and AWE in the ammonia synthesis system is directly discharged into the environment through cooling utilities, which will not affect the heat exchange process between system processes. The AWE and PEMEC synergistic hydrogen production scheme will have wide application potential in future ammonia synthesis systems. According to the fluctuation characteristics of renewable energy in different locations, it is expected to achieve a trade-off between the economy and flexibility of the ammonia synthesis system by optimizing the hydrogen production ratio of PEMEC and AWE.

Acknowledgments

This research has been supported by the Major Program of the National Natural Science Foundation of China (No.52090064).

Conflicts of Interest

The authors declare no conflict of interest. The funders had no role in the design of the study; in the collection, analyses, or interpretation of data; in the writing of the manuscript, or in the decision to publish the results.

References

[1] Wang L, Zhang Y, Pérez-Fortes M, Aubin P, Li n T-E, Yang Y, et al. Reversible solid-oxide cell sta ck based power-to-x-to-power systems: Compariso n of thermodynamic performance. Appl Energy 20 20 275:115330. https://doi.org/10.1016/j.apenergy. 2020.115330

[2] Cormos C-C. Deployment of integrated Power-t o-X and CO2 utilization systems: Techno-economi c assessment of synthetic natural gas and methanol cases. Appl Thermal Engin 2023 231:120943. https ://doi.org/10.1016/j.applthermaleng.2023.120943

[3] Nemmour A, Inayat A, Janajreh I, Ghenai C. Gr een hydrogen-based E-fuels (E-methane, E-methan ol, E-ammonia) to support clean energy transition: A literature review. Int J Hydro Energy 2023 48:29 011–33. https://doi.org/10.1016/j.ijhydene.2023.03. 240

[4] Giddey S, Badwal SPS, Munnings C, Dolan M. Ammonia as a Renewable Energy Transportation Media. ACS Sust Chem Eng 2017 5:10231–9. https ://doi.org/10.1021/acssuschemeng.7b02219

[5] Liu L, Duan L, Zheng N, Wang Q, Zhang M, X ue D. Thermodynamic performance evaluation of a novel solar-assisted multi-generation system driven by ammonia-fueled SOFC with anode outlet gas re circulation. Energy 2024 294:130845. https://doi.or g/10.1016/j.energy.2024.130845

[6] Bahnamiri FK, Khalili M, Pakzad P, Mehrpooy a M. Techno-economic assessment of a novel powe r-to-liquid system for synthesis of formic acid and a mmonia, based on CO2 electroreduction and alkali ne water electrolysis cells. Renewable Energy 2022 187:1224–40. https://doi.org/10.1016/j.renene.202 2.01.085

[7] Sousa J, Waiblinger W, Friedrich KA. Techno-e conomic Study of an Electrolysis-Based Green Am monia Production Plant. Ind Eng Chem Res 2022;6 1:14515–30. https://doi.org/10.1021/acs.iecr.2c003 83

[8] Richard S, Verde V, Kezibri N, Makhloufi C, S aker A, Gargiulo I, et al. Power-to-ammonia synthe sis process with membrane reactors: Techno- econo mic study. Int J Hydro Energy 2024 73:462–74. htt ps://doi.org/10.1016/j.ijhydene.2024.06.041

[9] Nowicki DA, Agnew GD, Irvine JTS. Green am monia production via the integration of a solid oxid e electrolyser and a Haber-Bosch loop with a series of solid electrolyte oxygen pumps. Energy Conver sion and Management 2023 280:116816. https://doi .org/10.1016/j.enconman.2023.116816

[10] Frattini D, Cinti G, Bidini G, Desideri U, Cioff i R, Jannelli E. A system approach in energy evalua tion of different renewable energies sources integra

tion in ammonia production plants. Renewable Energy 2016 99:472–82. https://doi.org/10.1016/j.renene.2016.07.040
[11] Nami H, Hendriksen PV, Frandsen HL. Green ammonia production using current and emerging electrolysis technologies. Renewable and Sustainable Energy Reviews 2024 199:114517. https://doi.org/10.1016/j.rser.2024.114517
[12] Zhou H, Chen Z, Meng W, Yang S. Design, global energy integration, and sustainability analyses of a process coupling renewable energy water electrolysis for hydrogen production with ammonia synthesis. J Env Chem Engin 2024 12:112892. https://doi.org/10.1016/j.jece.2024.112892
[13] Sánchez M, Amores E, Abad D, Rodríguez L, Clemente-Jul C. Aspen Plus model of an alkaline electrolysis system for hydrogen production. Int J Hydro Energy 2020 45:3916–29. https://doi.org/10.1016/j.ijhydene.2019.12.027
[14] Ulleberg O. Modeling of advanced alkaline electrolyzers: a system simulation approach. Int J Hydro Energy 2003 28:21–33. https://doi.org/10.1016/S0360-3199(02)00033-2
[15] Han B, Steen SM, Mo J, Zhang F-Y. Electrochemical performance modeling of a proton exchange membrane electrolyzer cell for hydrogen energy. Int J Hydro Energy 2015 40:7006–16. https://doi.org/10.1016/j.ijhydene.2015.03.164
[16] Aouali FZ, Becherif M, Ramadan HS, Emziane M, Khellaf A, Mohammedi K. Analytical modelling and experimental validation of proton exchange membrane electrolyser for hydrogen production. Int J Hydro Energy 2017 42:1366–74. https://doi.org/10.1016/j.ijhydene.2016.03.101
[17] Zheng N, Duan L, Wang X, Lu Z, Zhang H. Thermodynamic performance analysis of a novel PEMEC-SOFC-based poly-generation system integrated mechanical compression and thermal energy storage. Energy Conv Manag 2022 265:115770. https://doi.org/10.1016/j.enconman.2022.115770
[18] Yu J, Liu L, Du Y, Li Y, Zhang D, Li B, et al. Thermodynamic and Economic Analysis of the Green Ammonia Synthesis System Driven by Synergistic Hydrogen Production Using Alkaline Water Electrolyzers and Proton Exchange Membrane Electrolyzers. Energy Tech 2024 12:2401169. https://doi.org/10.1002/ente.202401169
[19] Debe MK, Hendricks SM, Vernstrom GD, Meyers M, Brostrom M, Stephens M, et al. Initial Performance and Durability of Ultra-Low Loaded NSTF Electrodes for PEM Electrolyzers. J Electrochem Soc 2012 159:K165. https://doi.org/10.1149/2.065206jes
[20] Zhang H, Wang L, Van herle J, Maréchal F, Desideri U. Techno-economic comparison of green ammonia production processes. Appl Energy 2020 259: 114135. https://doi.org/10.1016/j.apenergy.2019.114135
[21] Wang L, Rao M, Diethelm S, Lin T-E, Zhang H, Hagen A, et al. Power-to-methane via co-electrolysis of H2O and CO2: The effects of pressurized operation and internal methanation. Appl Energy 2019 250:1432–45. https://doi.org/10.1016/j.apenergy.2019.05.098
[22] Narasimhaiah G, Janardhanan VM. Modeling CO2 electrolysis in solid oxide electrolysis cell. J Solid State Electrochem 2013 17:2361–70. https://doi.org/10.1007/s10008-013-2081-8
[23] Araújo A, Skogestad S. Control structure design for the ammonia synthesis process. Computers & Chemical Engineering 2008 32:2920–32. https://doi.org/10.1016/j.compchemeng.2008.03.001
[24] Flórez-Orrego D, De Oliveira Junior S. Exergy assessment of single and dual pressure industrial ammonia synthesis units. Energy 2017 141:2540–58 https://doi.org/10.1016/j.energy.2017.06.139
[25] Kermani M, Wallerand AS, Kantor ID, Maréchal F. Generic superstructure synthesis of organic Rankine cycles for waste heat recovery in industrial processes. Appl Energy 2018 212:1203–25. https://doi.org/10.1016/j.apenergy.2017.12.094
[26] Zheng N, Zhang H, Duan L, Wang X, Wang Q, Liu L. Multi-criteria performance analysis and optimization of a solar-driven CCHP system based on PEMWE, SOFC, TES, and novel PVT for hotel and office buildings. Renew Energy 2023 206:1249–64. https://doi.org/10.1016/j.renene.2023.02.127